Journal of Quantum Science and Technology (JQST)

Vol.2 | Issue-4 | Issue Oct-Dec 2025| ISSN: 3048-6351 Online International, Refereed, Peer-Reviewed & Indexed Journal

Efficiency Enhancement of Monofacial and Bifacial PV Systems Under Realistic Shading Scenarios

DOI: https://doi.org/10.63345/jqst.v2i4.380

N. Pushparaju[1], Dr. J. Sreenivasulu[2], Dr. M. Anka Rao[3] & Dr. M. Rathaiah[4]

[1]M.Tech, EEE
JNTUA CEA
nallamala.pushparaju.pr@gmail.com

[2]Assistant Professor, EEE
JNTUA CEA
jsreenivasulu.eee@jntua.ac.in

[3]Assistant Professor, EEE
JNTUA CEA
ankaraomogili@gmail.com

[4]Assistant Professor, (Adhoc)
EEE, JNTUA CEA
ratnam355.eee@jntua.ac.in

ABSTRACT— Since 1950 onwards average 2% Human Population increases for every decade and matching bridge between electricity generation and demand is a big challenge. So, one of the prominent paths is to use Renewable Energy Sources (RES) like solar, wind etc. Solar energy is regarded as one of the most dependable energy sources for meeting future energy demands, as solar photovoltaic (PV) systems directly convert solar irradiation into electricity. However, the overall performance of PV systems can be impacted by various environmental factors. Key contributors to power losses include partial shading, hotspot formation, dust accumulation, and other similar issues., these factors can lead to mismatch losses which reduce power output. To mitigate these losses, PV modules are arranged in different array configurations, and their performance can differ based on environmental influences and the design of the configuration. This study explores several array layout strategies such as Total-Cross-Tied (TCT), Magic Square (McSq), and Dominant Square (DmSq), applied to both monofacial and bifacial PV systems. In Literature, it is identified that PV array configurations with shading patterns like Healthy, Corner, Center, L-Shape, Frame and Diagonal are considered for mono-facial PV System. But, Earth rotates around the sun. Hence, there is a chance of occurrence of new shading patterns like Row-wise, Column-wise and Diagonal strip shading. And recent developments in bifacial PV modules have garnered significant attention due to their increasing affordability and enhanced output compared to traditional monofacial solar panels. The advantage of bifacial technology lies in its ability to capture additional irradiance from the rear side, a feature that monofacial panels lack. This capability allows bifacial modules to generate more power, making them an appealing option for improving the efficiency of solar energy systems. Hence, it is motivated to consider Row-wise, Column-wise and Diagonal strip shading patterns for mono-facial and Bifacial too. This analysis utilizes a MATLAB/Simulink® model of a 5 × 5 PV

Journal of Quantum Science and Technology (JQST)

Vol.2 | Issue-4 | Issue Oct-Dec 2025| ISSN: 3048-6351 Online International, Refereed, Peer-Reviewed & Indexed Journal

array for each configuration, tested under various shading scenarios. The outcomes classify each configuration as consistent, optimal, average, or underperforming, aiding in the selection of the most suitable configuration for particular environmental conditions.

Keywords— Partial Shading, Array Configurations, Bifacial Photovoltaic System, Mismatch loss reduction.

1. INTRODUCTION:

Solar energy stands out as the most dependable source to meet future energy needs [1]. The two main approaches for capturing solar energy are solar thermal collection and photovoltaic conversion. Thermal systems harness heat from the sun, whereas PV systems generate electricity by converting sunlight through the photovoltaic effect [2]. The primary causes of power loss include: i) partial shading [3] ii) hotspots, iii) temperature variations [4], iv) module delamination [5], v) accumulation of dust on the panel surface [6], [7] etc. Partial shading is an unpredictable event that can lead to significant power losses in photovoltaic systems. Figure 1 illustrates the various factors responsible for partial shading. To mitigate the development of hotspots, bypass diodes are incorporated into PV modules [8].

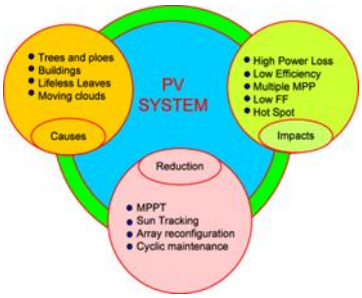

Figure 1: Causes, Impacts and Reduction of Partial shading in PV System

Hotspots occur when current is forced through shaded or damaged cells, causing a rise in their operating temperature. Overheating causes certain PV cells to operate like resistive loads, compromising the performance of nearby cells. Bypass diodes are therefore added in parallel to redirect current around these compromised cells, ensuring continued array performance. Compared to fixed array configurations, reconfiguration methods involve higher implementation and operational costs. The paper thoroughly analyzes these methods by examining their efficiency, dependability, durability, ease of implementation, practical relevance, and the benefits and drawbacks linked to each.

Traditional photovoltaic panels, known as monofacial panels, generate electricity by absorbing sunlight solely on their front surface. Unlike monofacial modules, bifacial PV modules are engineered to absorb solar irradiance from both their front and back surfaces, leading to higher energy generation. The concept of bifacial solar technology was first introduced in the 1960s as a means to improve the efficiency of photovoltaic systems. Its development gained significant momentum in the 1980s when a team of researchers from Spain demonstrated notable improvements in efficiency and energy gain using bifacial cells. Since then, bifacial modules have been recognized for their potential to deliver higher energy yields compared to conventional monofacial panels, while also supporting cost-effective implementation. The operational principle of the Bifacial PV system is illustrated in Figure 2.

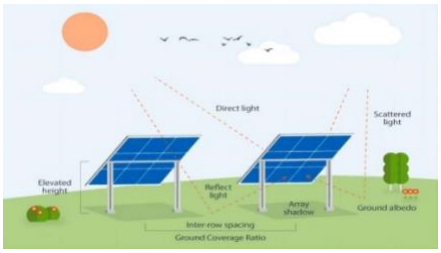

Figure 2: Working of the Bifacial PV System

The combination of view factor and tilt angle influences the amount of ground-reflected light that reaches the rear surface of a bifacial panel. By optimizing the tilt and elevation, rear-side irradiance can be enhanced, thereby increasing the overall energy yield.

Journal of Quantum Science and Technology (JQST)

Vol.2 | Issue-4 | Issue Oct-Dec 2025| ISSN: 3048-6351 Online International, Refereed, Peer-Reviewed & Indexed Journal

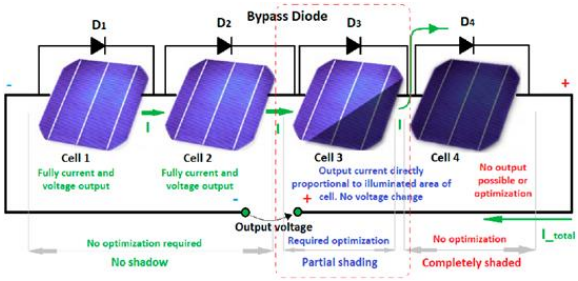

2. MATHEMATICAL MODELING:

An essential aspect of evaluating the performance of a PV system is the precise mathematical modeling of the PV cell. The single-diode model is widely recognized as one of the most frequently applied methods for this purpose [9]. This approach simulates the PV cell through an equivalent circuit comprising a current source, a parallel-connected diode, and both series and shunt resistances. The schematic of this model is illustrated in Figure 3. The maximum current output (I_m) from the PV cell using the single-diode model is defined by the equation:

$$I_m = I_L - I_D - I_{sh}$$

Here, I_m represents the peak current generated by the cell, I_L is the current produced by incident light, and I_D is the diode current. The power output (P_m) from the PV cell can then be expressed as:

$$P_m = I_m \times V_m$$

Where V_m is the voltage at maximum power point, and Im is the corresponding maximum current.

The *Fill Factor* (FF), an important parameter for evaluating the efficiency of a PV module, is determined by the relationship between the maximum voltage (V_m), maximum current (I_m), open-circuit voltage (V_{OC}), and short-circuit current (I_{SC}). It is mathematically expressed as:

Figure 3: Single diode model and Causes of Partial shading scenarios

$$FF = (V_m \times I_m) / (V_{OC} \times I_{SC})$$

Using this, the maximum power output (P_m) of a PV module can be derived with the following formula:

$$P_m = (V_{OC} \times I_{SC}) \times FF$$

These core equations serve as the foundation for simulating and analyzing the behavior of PV arrays. Under standard test conditions (1000 W/m²), the solar panel operates at its rated current output. However, when the irradiance drops to lower levels, such as 100 W/m², the current output decreases significantly down to nearly 10% of the rated value. A MATLAB/Simulink®. Simulation model is used to study the impact of varying irradiance levels on power generation. The resulting P-V (Power vs. Voltage) and I-V (Current vs. Voltage) curves, generated demonstrate the performance response of the PV system under fluctuating irradiance conditions. The efficiency of a PV cell is defined as the ratio between its actual power output to the cell's specified rated power. This relationship is mathematically expressed as follows:

$$\text{Efficiency, } \eta = P_m / P_{STC} \times 100\%$$

In bifacial PV systems, electricity is produced from both the front and back surfaces of the module. The front surface captures direct sunlight, whereas the rear surface utilizes light reflected off the ground. The contribution of this reflected light is quantified by rear irradiance (G_{rear}), which is influenced by three key factors: the albedo (ρ) of the ground surface, the front-side irradiance (G_{front}), and the view factor (F_{view}), which represents how much of the reflected light reaches the rear surface. This relationship is expressed as:

$$G_{rear} = \rho \cdot G_{front} \cdot F_{view}$$

However, since the rear side of bifacial panels is typically less efficient than the front, its contribution is scaled using the Bifaciality factor (ϕ), leading to the total effective irradiance input for energy generation:

$$G_{total} = G_{front} + \phi \cdot G_{rear}$$

These equations form the foundation for modeling and simulation of bifacial PV system performance under various ground conditions and mounting setups. [10]

Albedo: Albedo refers to the ratio of light that is reflected from a surface compared to the incident radiation. It ranges from 0% (no light reflection) to 100% (perfect reflection). A higher

albedo means more reflected light reaches the backside of a bifacial PV module, which increases its power generation. Albedo = Reflected Light / Incident Light

According to the material and surface, the albedo values are shown in Table 1 [11] and Table 2 [12] respectively.

Table 1: Material and its Reflectance

Material	Reflectance* (R)	G_{rear} at 1000 W/m² front
Asphalt	0.1	70 W/m²
Light Soil	0.21	130 W/m²
Concrete	0.28	170 W/m²
Beige built-up roofing	0.43	250 W/m²
White EDPM roofing	0.8	430 W/m²

Table 2: Surface and its Albedo

Surface	Albedo
Grass	0.15-0.25
Fresh snow	0.82
Wet snow	0.55-0.75
Dry Asphalt	0.09-0.15
Concrete	0.25-0.35
Aluminum	0.85
New galvanized steel	0.35
Very dirty galvanized	0.08

View Factor: The view factor (or configuration factor) represents the portion of sunlight reflected from the ground that is captured by the rear side of a bifacial PV panel. It is a dimensionless value ranging from 0 to 1, where:

- 0 means the panel sees no ground (no reflected light reaches the rear),
- 1 means the panel sees the entire ground below it (maximum reflected light reaches the rear).

The typical view factor values for various mounting conditions is shown in Table 3.

Table 3: Mounting conditions and its View Factor

Mounting Condition	Typical View Factor
Flat mounting	0.1-0.2
Moderate tilt and height	0.3-0.5
High ground clearance(canopy)	0.6-0.8

Tilt angle: Tilt angle refers to the angle between the surface of the PV panel and the horizontal ground plane**.** It determines the panel's orientation toward the sun and plays a key role in how much solar radiation it can collect.

- Tilt angle = 0°: panel is flat (horizontal)
- Tilt angle = 90°: panel is vertical (e.g., on a wall)

The effects for various tilt angle is shown in Table 4.

Table 4: Tilt angle and its effect

Tilt Angle	Effect
0° (flat)	Front side gets less direct sunlight; rear gets minimal reflection.
20°-30° (optimal)	Balances front-side generation and rear-side view factor.
90° (vertical)	Front side gets sunlight only during morning/evening; rear gets very little reflection (low view factor).

3. SIMULINK MODEL OF DIFFERENT ARRAY CONFIGURATIONS:

A 5 x 5 matrix formation of different array configurations are modeled in MATLAB/*SIMULINK*® are shown in figure 4.

V

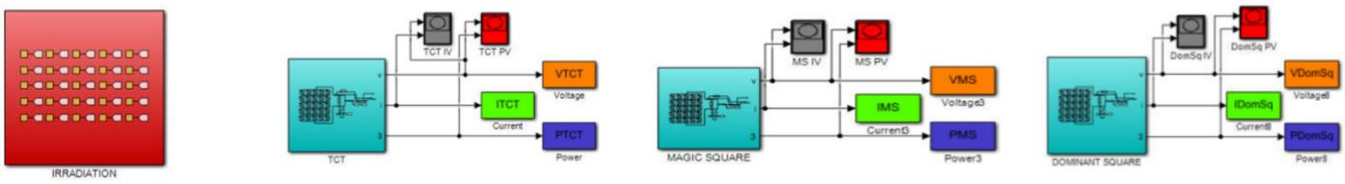

Figure 4: Simulation diagram of the various array configurations.

The PV module specifications are outlined in Table 5. The power output and efficiency were evaluated for different array configurations, including the TCT, McSq, and DmSq arrangements. MATLAB/SIMULINK® was employed to simulate and compute the power generation and efficiency for each of these configurations. All the array configurations are implemented in a 5×5 matrix layout, with each PV cell modelled using the single-diode approach, as illustrated in Figure 8. The P-V (Power-Voltage) and I-V (Current-Voltage) characteristic curves were obtained using the Data Inspector feature in MATLAB/SIMULINK®. X-axis scale is 20volts and Y-axis scale is 200W & X-axis scale is 20volts and Y-axis scale is 2 Amps are the limits for P-V & I-V characteristics. Various shading patterns were applied, reflecting the non-uniform solar exposure PV panels experience throughout the day.

Table 5: Ratings of PV modules

S.No.	Parameters	Rating
1.	P_m – Maximum Power	213.15Wp
2.	V_m – Maximum Power Voltage	29V
3.	I_m – Maximum Power Current	7.35A
4.	I_{SC} – Short Circuit Current	7.84A
5.	V_{OC} – Open Circuit Voltage	36.3V
6.	G_{STC} – STC Irradiance	1000W/m^2
7.	T_{STC} – STC Temperature	25^{0}C

Each panel in the simulation receives irradiation data from a block containing 25 different irradiation values. These parameters are assigned to individual subsystems within the array configurations through the use of Goto blocks. Simulations are carried out under varying shading conditions, reflecting the non-uniform solar exposure experienced by PV panels throughout the day. The level of irradiation fluctuates over time, which is natural because, the nature of these shading patterns is often inconsistent and unpredictable. In PV systems, uneven solar exposure—commonly referred to as partial shading—may result from external factors like surrounding trees, buildings, towers, cloud cover, and other obstacles. Such partial shading causes certain rows in the PV array to generate unequal currents, resulting in mismatch losses. These losses indicate the variation in power output between the most efficient and the least efficient rows. As a result, the power generation of healthy modules is compromised by the weaker ones, leading to reduced overall efficiency due to mismatch losses. To assess the performance of each configuration, common shading scenarios such as Corner, Center, L-Shape, Frame, and Diagonal were used in the simulation, as demonstrated in [13]. After completing the analysis of the various shading patterns mentioned in the reference paper, additional shading scenarios—such as, Row-wise, Column-wise, and Diagonal strip shading. These shading patterns, as shown in Figure 5, expose the PV modules to different levels of solar irradiance.

3.1 TYPES OF SHADING PATTERNS:

1.Row-Wise:

a. Row-1:

• PV11 receives 800 W/m²,
• PV12 receives 400 W/m²,
• PV13 receives 900 W/m²,
• PV14 receives 600 W/m²,
• PV15 receives 200 W/m²,
while the remaining modules operate under uniform irradiance of 1000 W/m².

b. Two-rows:

• PV11 and PV24 receives 800 W/m²,
• PV12 and PV22 receives 400 W/m²,
• PV13 and PV25 receives 900 W/m²,
• PV14 and PV23 receives 600 W/m²,
• PV15 and PV21 receives 200 W/m²,
while the remaining modules operate under uniform irradiance of 1000 W/m².

c. Three-rows:

• PV11, PV24 and PV31 receives 800W/m^2.
• PV12, PV22 and PV34 receives 400W/m^2
• PV13, PV25 and PV32 receives 900W/m^2
• PV14, PV23 and PV35 receives 600W/m^2
• PV15, PV21 and PV33 receives 200W/m^2
while the remaining modules operate under uniform irradiance of 1000 W/m^2.

d. Four-rows:
• PV11, PV24, PV31 and PV43 receives 800W/m^2.
• PV12, PV22, PV34 and PV45 receives 400W/m^2
• PV13, PV25, PV32 and PV44 receives 900W/m^2
• PV14, PV23, PV35 and PV41 receives 600W/m^2
• PV15, PV21, PV33 and PV42 receives 200W/m^2
while the remaining modules operate under uniform irradiance of 1000 W/m^2.

e. Five-rows:
• PV11, PV24, PV31, PV43 and PV55 receives 800W/m^2.
• PV12, PV22, PV34, PV45 and PV53 receives 400W/m^2
• PV13, PV25, PV32, PV44 and PV51 receives 900W/m^2
• PV14, PV23, PV35, PV41 and PV54 receives 600W/m^2
• PV15, PV21, PV33, PV42 and PV52 receives 200W/m^2.

2. Column-wise:
a. Column-1:
• PV11 receives 800 W/m^2,
• PV12 receives 400 W/m^2,
• PV13 receives 900 W/m^2,
• PV14 receives 600 W/m^2,
• PV15 receives 200 W/m^2,
while the remaining modules operate under uniform irradiance of 1000 W/m^2.

b. Two-columns:
• PV11 and PV24 receives 800 W/m^2,
• PV12 and PV22 receives 400 W/m^2,
• PV13 and PV25 receives 900 W/m^2,
• PV14 and PV23 receives 600 W/m^2,
• PV15 and PV21 receives 200 W/m^2,
while the remaining modules operate under uniform irradiance of 1000 W/m^2.

c. Three Columns:
• PV11, PV24 and PV31 receives 800W/m^2.
• PV12, PV22 and PV34 receives 400W/m^2
• PV13, PV25 and PV32 receives 900W/m^2
• PV14, PV23 and PV35 receives 600W/m^2
• PV15, PV21 and PV33 receives 200W/m^2
while the remaining modules operate under uniform irradiance of 1000 W/m^2.

d. Four-columns:
• PV11, PV42, PV13 and PV34 receives 800W/m^2.
• PV21, PV22, PV43 and PV54 receives 400W/m^2
• PV31, PV52, PV23 and PV44 receives 900W/m^2
• PV41, PV32, PV53 and PV14 receives 600W/m^2
• PV51, PV12, PV33 and PV24 receives 200W/m^2

while the remaining modules operate under uniform irradiance of 1000 W/m^2.

e. Five-columns:
• PV11, PV24, PV31, PV43 and PV55 receives 800W/m^2.
• PV12, PV22, PV34, PV45 and PV53 receives 400W/m^2
• PV13, PV25, PV32, PV44 and PV51 receives 900W/m^2
• PV14, PV23, PV35, PV41 and PV54 receives 600W/m^2
• PV15, PV21, PV33, PV42 and PV52 receives 200W/m^2.

3. Diagonal strip shading:
a. 1st Diagonal strip:
• PV11 receives 200 W/m^2
while the remaining modules operate under uniform irradiance of 1000 W/m^2.

b. Two-Diagonal strips:
• PV11 and PV21 receives 200W/m^2.
• PV12 receives 400W/m^2.
while the remaining modules operate under uniform irradiance of 1000 W/m^2.

c. Three- Diagonal strips:
• PV11 and PV21 receives 200W/m^2

• PV12 and PV31 receives 400W/m^2
• PV22 receives 600W/m^2
• PV13 receives 800W/m^2
while the remaining modules operate under uniform irradiance of 1000 W/m^2.

d. Four- Diagonal strips:

e. Five- Diagonal strips:

• PV11 and PV21 receives 200W/m^2
• PV12, PV31 and PV32 receives 400W/m^2
• PV22, PV41, PV42 and PV24 receives 600W/m^2
• PV13, PV23, PV51 and PV33 receives 800W/m^2
• PV14 and PV15 receives 900W/m^2
while the remaining modules operate under uniform irradiance of 1000 W/m^2.

3.2 POSITION-BASED SHADING PATTERNS:

Various position-based shading scenarios, such as Healthy, Corner, and Center, were evaluated for the Bifacial PV system

• PV11 and PV21 receives 200W/m^2
• PV12, PV31 and PV32 receives 400W/m^2
• PV22 and PV41 receives 600W/m^2
• PV13 and PV23 receives 800W/m^2
• PV14 receives 900W/m^2
while the remaining modules operate under uniform irradiance of 1000 W/m^2.
[13]. These shading scenarios illustrated in Figure 6, the PV modules experience varying levels of solar irradiance.

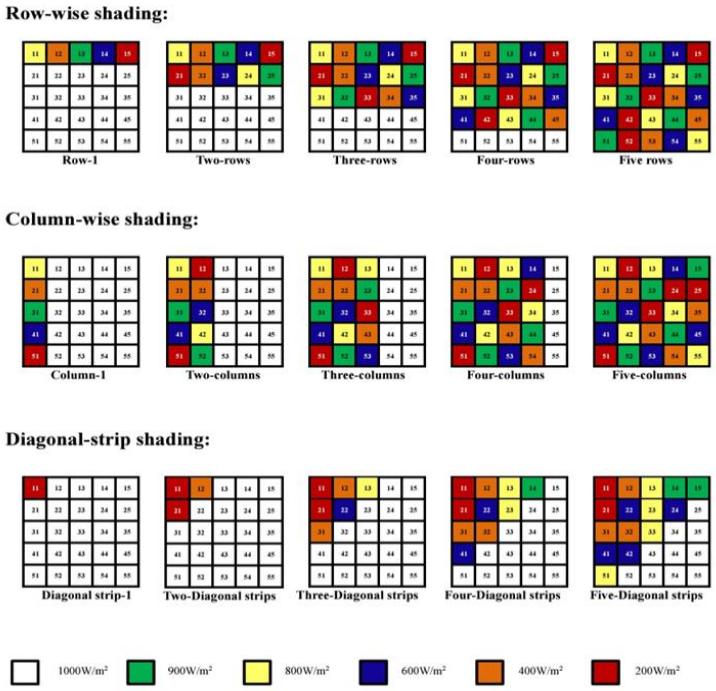

Figure 5: Various kinds of shading patterns used for the analysis

a. HEALTHY PATTERN:

In this shading pattern, all modules in the 5×5 PV array are exposed to uniform irradiance of 1000 W/m^2.

b. CORNER SHADING PATTERN:

• PV15 receives 900 W/m^2,
• PV11 and PV55 receives 800 W/m^2,

Journal of Quantum Science and Technology (JQST)
Vol.2 | Issue-4 | Issue Oct-Dec 2025| ISSN: 3048-6351 Online International, Refereed, Peer-Reviewed & Indexed Journal

• PV51 receives 400 W/m²,
while the remaining modules operate under uniform irradiance of 1000 W/m².

c. CENTRE SHADING PATTERN:
• PV43 receives 900 W/m²,
• PV32 and PV44 receives 800 W/m²,

d. FRAME SHADING PATTERN:
• PV31 receives 900 W/m²,
• PV11 and PV55 receives 800 W/m²,
• PV21 and PV53 receives 600 W/m²,
• PV51 and PV54 receives 400 W/m²,
while the remaining modules operate under uniform irradiance of 1000 W/m².

e. DIAGONAL SHADING PATTERN:
• PV55 receives 900 W/m²,
• PV44 receives 800 W/m²,
• PV33 receives 600 W/m²,
• PV22 receives 400 W/m²,
• PV24 and PV42 receives 600 W/m²,
• PV23 and PV34 receives 400 W/m²,
• PV22 and PV33 receives 200 W/m²,
while the remaining modules operate under uniform irradiance of 1000 W/m².

• PV11 receives 200 W/m²,
while the remaining modules operate under uniform irradiance of 1000 W/m².

4. SIMULINK MODEL FOR MONOFACIAL PV SYSTEM:

The monofacial PV system comprises 25 solar modules arranged using the TCT connection scheme across all array configurations. The matrix layouts for the TCT, McSq and DmSq configurations are illustrated in Figure 7. This setup provides three output parameters: Maximum Power Output (P_m), Open-circuit Voltage (V_{OC}), and Short-circuit Voltage (I_{SC}). Discrete values of these parameters are transferred to the workspace for comparative analysis. The P-V and I-V characteristics are plotted using the Data Inspector tool in MATLAB/*SIMULINK*®.

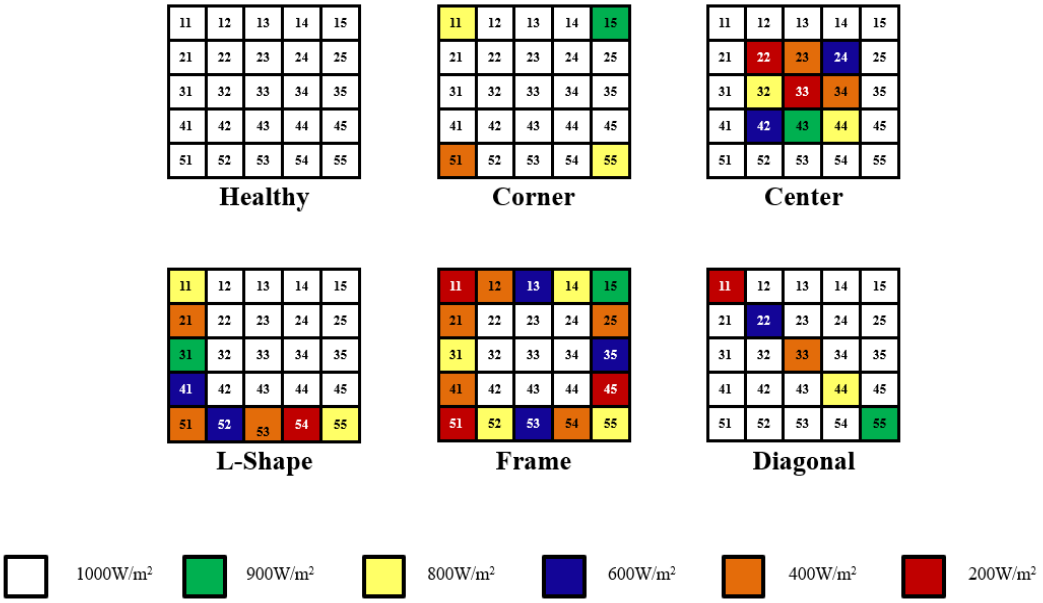

Figure 6: Various kinds of Position-Based Shading Scenarios

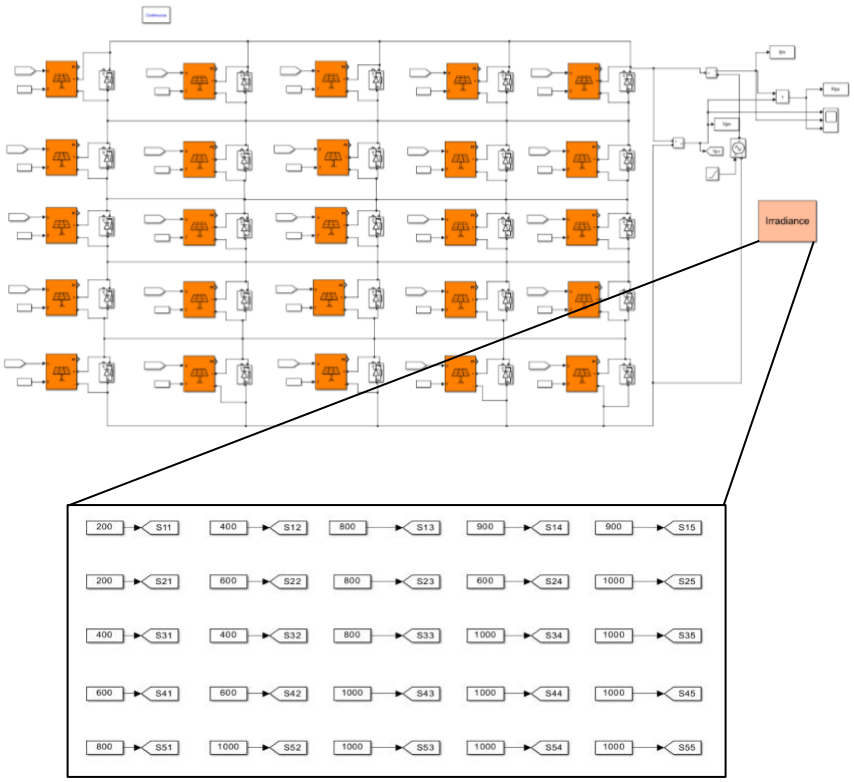

Figure 7: Array Configuration for Monofacial PV System

11	12	13	14	15
21	22	23	24	25
31	32	33	34	35
41	42	43	44	45
51	52	53	54	55

For TCT

11	32	53	24	45
42	13	34	55	21
23	44	15	31	52
54	25	41	12	33
35	51	22	43	14

For McSq

42	54	22	45	13
14	32	55	23	41
31	15	33	51	24
25	43	11	34	52
53	21	44	12	35

For DmSq

Figure 8: Matrix Diagrams of 5x5 PV arrays under different configurations

Journal of Quantum Science and Technology (JQST)

Vol.2 | Issue-4 | Issue Oct-Dec 2025| ISSN: 3048-6351 Online International, Refereed, Peer-Reviewed & Indexed Journal

4.1 TOTAL-CROSS-TIED(TCT):

In the TCT array configuration, PV modules are connected in both series and parallel with neighboring modules, as depicted in Figure 7. The corresponding P-V and I-V characteristic curves under row-wise, column-wise and diagonal-strip shading are illustrated in 9.1, 9.2, 9.3 respectively.

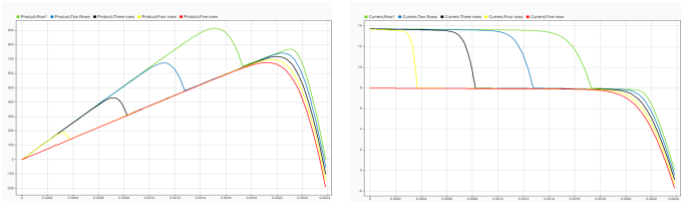

Figure 9.1 Characteristic graphs of the TCT arrangement under row-wise shading pattern

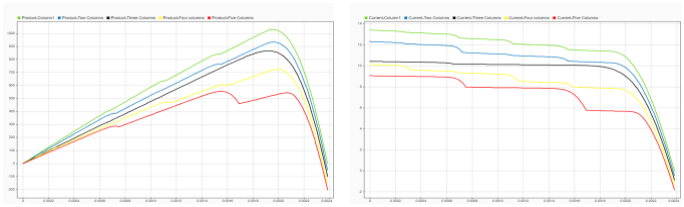

Figure 9.2 Characteristic graphs of the TCT arrangement under column-wise shading pattern.

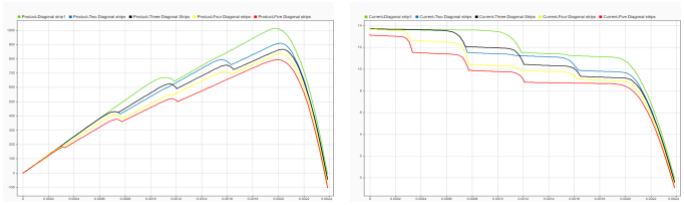

Figure 9.3 Characteristic graphs of the TCT arrangement under Diagonal-strip shading pattern

4.2 MAGIC SQUARE (McSq):

To enhance power extraction, the McSq configuration is employed, which is based on a numerical logic where the numbers from 1 to n re organized in an $n \times n$ matrix such that each row, column, and diagonal has an equal sum. The corresponding PV array layout following this magic square principle is also depicted in Figure 7. This structured design helps reduce mismatch losse matrix so that the sums of all rows, columns, and diagonals are equal. The electrical performance of a 5×5 McSq array under row-wise, column-wise and diagonal-strip shading patterns are demonstrated through the P-V and I-V plots in Figures10.1, 10.2, and 10.3 respectively.

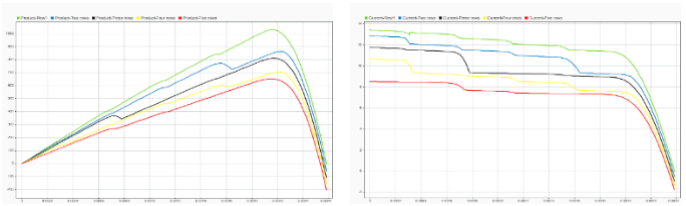

Figure 10.1 Characteristic graphs of the McSq arrangement under row-wise shading pattern.

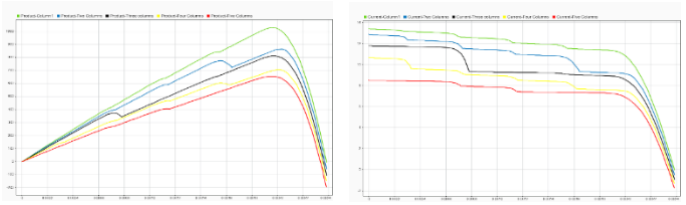

Figure 10. Characteristic graphs of the McSq arrangement under column-wise shading pattern.

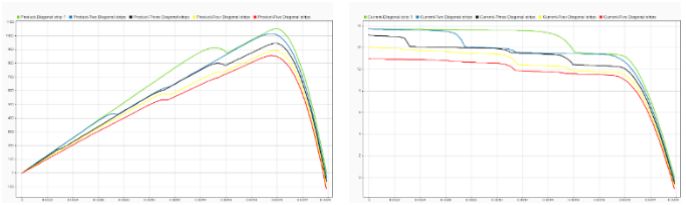

Figure 10.3 Characteristic graphs of the McSq arrangement under Diagonal-strip shading pattern.

Journal of Quantum Science and Technology (JQST)

Vol.2 | Issue-4 | Issue Oct-Dec 2025| ISSN: 3048-6351 Online International, Refereed, Peer-Reviewed & Indexed Journal

4.3 DOMINANCE SQUARE (DmSq):

The DmSq array configuration, originally introduced in [14], urther enhances PV array performance. It modifies the conventional TCT layout by repositioning modules within each row and column based on dominance square logic. The matrix structure of this configuration is shown in Figure 7 and its P-V and I-V curves under row-wise, column-wise and diagonal-strip shading conditions are displayed in Figures 11.1,11.2,11.3 respectively

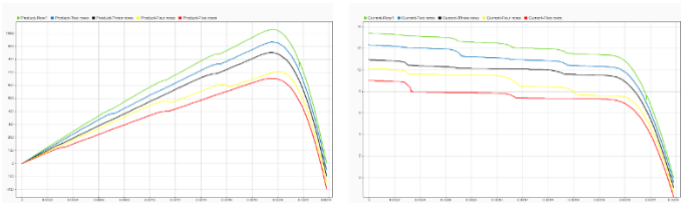

Figure 11.1 Characteristic graphs of the DmSq arrangement under row-wise shading pattern

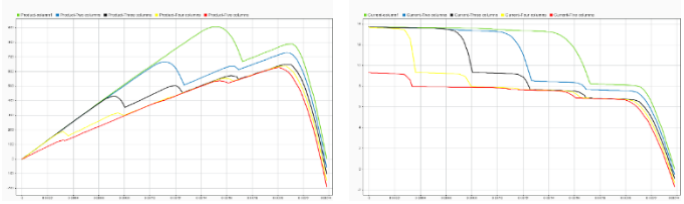

Figure 11.2 Characteristic graphs of the DmSq arrangement under column-wise shading pattern

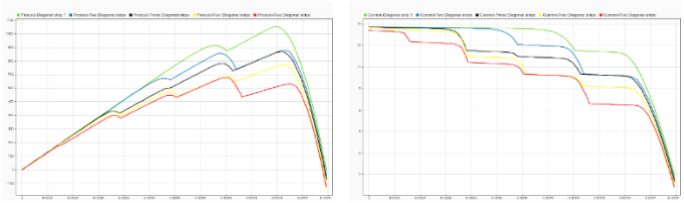

Figure 11.3 Characteristic graphs of the DmSq arrangement under Diagonal-strip shading pattern.

The bifacial PV System consists of 25 PV array modules, which are connected in TCT connections for all types of array configurations. The Matrix formation for TCT, McSq, DmSq is shown in figure 7. The system is classified as a Bifacial PV System due to the integration of rear-side and front-side irradiance, with the resultant total irradiance supplied to the primary irradiance input of the PV module. The irradiance summation is implemented within a dedicated subsystem, as shown in figure 13.

5.1 TOTAL-CROSS-TIED(TCT):

For bifacial PV systems, the TCT configuration is illustrated in Figure 13. Various shading patterns—such as row-wise, column-wise, and diagonal-strip—are applied to assess performance. The corresponding characteristic curves for a 5×5 bifacial array are presented in Figure 12.1 for row-wise shading, Figure 12.2 for column-wise shading, and Figure 12.3 for diagonal-strip shading.

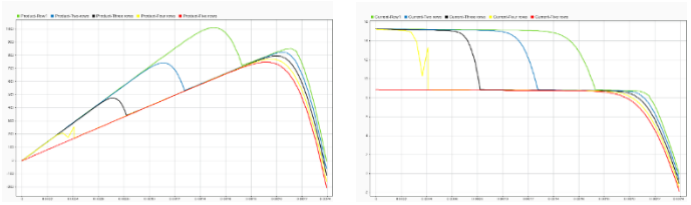

Figure 12.1 Characteristic graphs of the TCT arrangement under row-wise shading pattern.

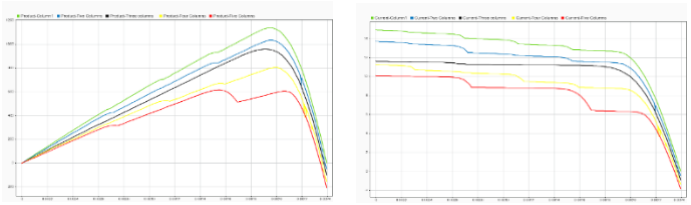

Figure 12.2 Characteristic graphs of the TCT arrangement under column-wise shading pattern.

5. SIMULINK MODEL FOR BIFACIAL PV SYSTEM:

Journal of Quantum Science and Technology (JQST)

Vol.2 | Issue-4 | Issue Oct-Dec 2025| ISSN: 3048-6351 Online International, Refereed, Peer-Reviewed & Indexed Journal

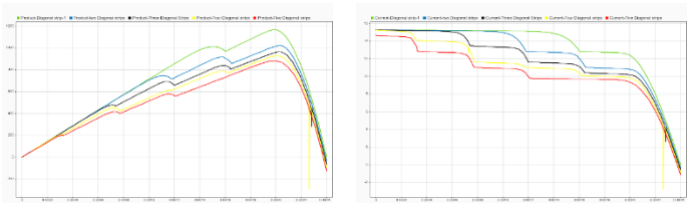

Figure 12.3 Characteristic graphs of the TCT arrangement under Diagonal-strip shading pattern.

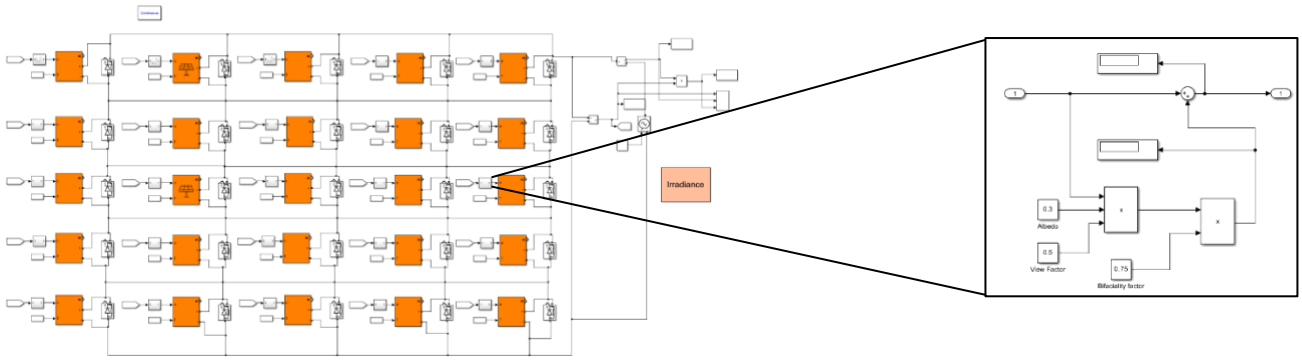

Figure 13: Array Configuration for Bifacial PV System

5.2 MAGIC SQUARE (McSq):

The McSq array configuration for the bifacial PV system is illustrated in Figure 13 Various shading patterns—row-wise, column-wise, and diagonal-strip—are applied, and the corresponding performance curves for the 5×5 array are shown in Figure 14.1 (row-wise), Figure 14.2 (column-wise), and Figure 14.3 (diagonal-strip).

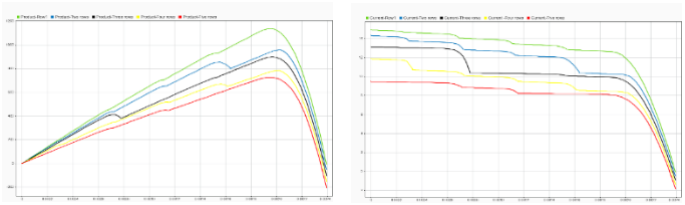

Figure 14.1 Characteristic graphs of the McSq arrangement under row-wise shading pattern.

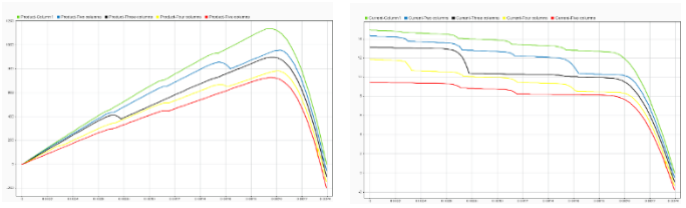

Figure 14.2 Characteristic graphs of the McSq arrangement under column-wise shading pattern.

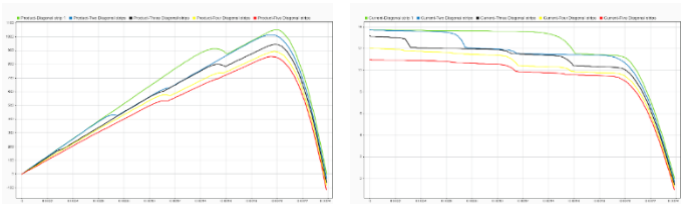

Figure 14.3 Characteristic graphs of the McSq arrangement under Diagoanl-strip shading pattern.

5.3 DOMINANT SQUARE (DmSq):

The DmSq array configuration is illustrated in the figure 13, is evaluated under the same shading scenarios. The resulting P-V and I-V characteristic curves are presented in Figures 15.1, 15.2,

15.3 for row-wise, column-wise, and diagonal-strip shading, respectively.

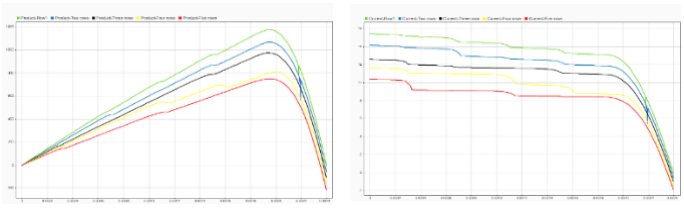

Figure 15.1 Characteristic graphs of the DmSq arrangement under row-wise shading pattern.

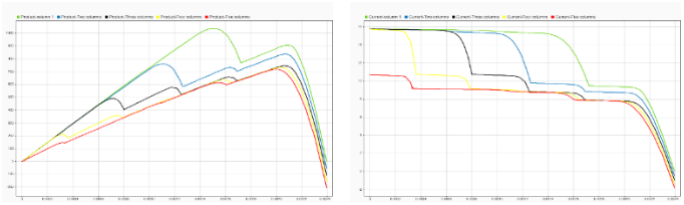

Figure 15.2 Characteristic graphs of the Dmsq arrangement under column-wise shading pattern.

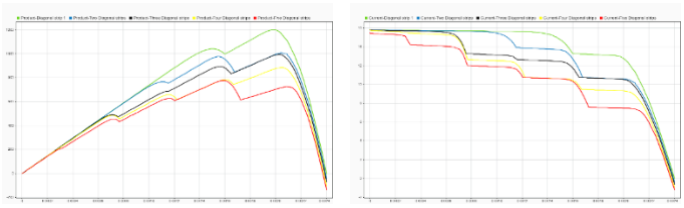

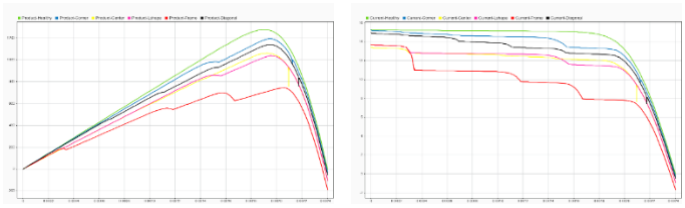

Figure 17: Characteristic graphs of the McSq arrangement under position-based shading patterns.

Figure 15.3 Characteristic graphs of the DmSq arrangement under Diagonal-strip shading pattern.

6. POSITION BASED SHADING PATTERNS FOR BIFACIAL PV ARRAY:

6.1 TOTAL-CROSS-TIED(TCT):

A 5×5 PV array configured using the TCT method is assessed under different position-based shading conditions. The related P-V and I-V curves are provided in Figure 16. Under uniform irradiance (healthy condition), the TCT array achieves its rated power output.

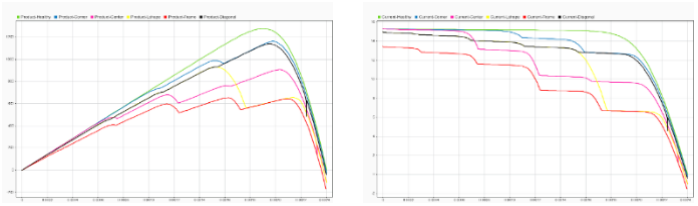

Figure 16: Characteristic graphs of the TCT arrangement under position-based shading patterns.

6.2 MAGIC SQUARE (McSq):

The performance of the McSq configuration under varying shading patterns is illustrated in Figure 17 through its P-V and I-V characteristics. While the array delivers rated power output under standard test conditions, its output decreases when exposed to shading. Nonetheless, the McSq configuration exhibits superior performance compared to other array configurations.

The DmSq array configuration is introduced to improve the efficiency of the solar PV array. Its P-V and I-V characteristic curves under different shading conditions are illustrated in Figure 18.

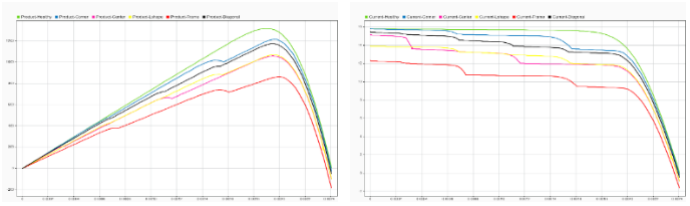

6.3 DOMINANT SQUARE (DmSq):

Figure 18: Characteristic graphs of the DmSq arrangement under position-based shading patterns.

7. RESULTS AND DISCUSSIONS:

In this paper, the performance of monofacial and bifacial PV systems was evaluated under different partial shading patterns, using three array configurations: TCT, McSq and DmSq

7.1 FOR MONOFACIAL PV ARRAY:

Analysis of different PV array configurations affected by ROW-WISE shading:

Array Configuration	Output	Row-1	Two-rows	Three-rows	Four rows	Five rows
TCT	Isc (A)	13.8	13.8	13.8	13.7	8.0
	Power (W)	913.4	741.2	716.9	694.9	674.6
	Efficiency (%)	79.10	64.19	62.09	60.18	58.42
McSq	Isc (A)	13.5	12.9	11.8	10.7	8.5
	Power (W)	1029.0	862.2	810.8	704.8	651.6
	Efficiency (%)	89.11	74.66	70.21	61.03	56.43
DmSq	Isc (A)	13.5	12.4	11.0	10.2	9.1
	Power (W)	1028.0	932.5	851.4	706.0	654.0
	Efficiency (%)	89.03	80.76	73.73	61.14	56.64

Analysis of different PV array configurations affected by COLUMN-WISE shading:

Array Configuration	Output	Column-1	Two- Columns	Three-Columns	Four-Columns	Five- Columns
TCT	Isc (A)	13.5	12.4	10.4	10.2	9.1
	Power (W)	1028.8	**932.6**	**865.3**	**723.7**	554.3
	Efficiency (%)	89.10	80.77	74.94	62.67	48.00
McSq	Isc (A)	13.5	12.9	11.8	10.7	8.5

	Power (W)	**1028.8**	863.9	811.3	705.4	**654.0**
	Efficiency (%)	89.09	74.81	70.26	61.08	56.63
DmSq	**Isc (A)**	13.8	13.8	13.8	13.7	9.3
	Power (W)	908.2	729.5	649.4	637.7	627.2
	Efficiency (%)	78.65	63.18	56.24	55.23	54.32

Analysis of different PV array configurations affected by DIAGONAL-STRIP shading:

Array Configuration	Output	Diagonal-strip 1	Two-Diagonal-strips	Three-Diagonal-strips	Four-Diagonal-strips	Five-Diagonal-strips
TCT	**Isc (A)**	13.8	13.8	13.8	13.7	13.2
	Power (W)	1014.3	911.2	868.4	835.4	794.0
	Efficiency (%)	87.84	78.91	75.21	72.35	68.76
McSq	**Isc (A)**	13.8	13.8	13.2	12.1	11.0
	Power (W)	1052.4	**1014.4**	**946.6**	**893.4**	**856.2**
	Efficiency (%)	91.14	87.84	81.97	77.37	74.14
DmSq	**Isc (A)**	13.8	13.8	13.8	13.7	13.5
	Power (W)	**1053.3**	879.6	869.4	771.7	678.8
	Efficiency (%)	91.22	76.18	75.29	66.83	58.79

7.2 FOR BIFACIAL PV ARRAY:

Analysis of different PV array configurations affected by ROW-WISE shading:

Array Configuration	Output	Row-1	Two-rows	Three-rows	Four rows	Five rows
TCT	**Isc (A)**	15.3	15.3	15.3	15.3	8.9
	Power (W)	1001.4	823.5	796.2	771.6	748.9
	Efficiency (%)	79.09	64.46	62.32	60.40	58.62
McSq	**Isc (A)**	15	14.4	13.2	11.9	9.5
	Power (W)	1139.5	958.8	899.9	784.5	727.1
	Efficiency (%)	89.21	75.06	70.45	61.41	56.92
DmSq	**Isc (A)**	15.5	14.2	12.6	11.7	10.4
	Power (W)	**1176.0**	**1066.8**	**974.4**	**810.1**	**750.4**
	Efficiency (%)	89.23	80.95	73.94	61.47	56.94

Analysis of different PV array configurations affected by COLUMN-WISE shading:

Array Configuration	Output	Column-1	Two-Columns	Three-Columns	Four-Columns	Five- Columns
TCT	**Isc (A)**	15.0	13.7	11.6	11.3	10.1

	Power (W)	**1139.6**	**1033.7**	**958.7**	**804.0**	615.6
	Efficiency (%)	89.21	80.92	75.05	62.94	418.19
MS	**Isc (A)**	15.0	14.4	13.2	11.9	9.5
	Power (W)	1139.3	958.4	900	784.4	**727.9**
	Efficiency (%)	89.19	75.03	70.46	61.41	56.98
DS	**Isc (A)**	15.8	15.8	15.8	15.8	10.7
	Power (W)	1036.3	837.9	746.8	734.1	720.5
	Efficiency (%)	78.63	63.58	56.67	55.70	54.67

Analysis of different PV array configurations affected by DIAGONAL-STRIP shading:

Array Configuration	Output	Diagonal-strip 1	Two-Diagonal-strips	Three-Diagonal-strips	Four-Diagonal-strips	Five-Diagonal-strips
TCT	**Isc (A)**	15.3	15.3	15.3	15.3	14.7
	Power (W)	1166.8	1021.1	963.4	927.2	880.7
	Efficiency (%)	91.34	79.93	75.41	72.58	68.94
MS	**Isc (A)**	15.3	15.3	14.7	13.4	12.2
	Power (W)	1165.9	**1124.7**	**1050.3**	**990.6**	**949.6**
	Efficiency (%)	91.27	88.05	82.22	77.55	74.34
DS	**Isc (A)**	15.8	15.8	15.8	15.8	15.5
	Power (W)	**1203.0**	1008.1	996.3	886.8	777.7
	Efficiency (%)	91.28	76.49	75.60	67.29	59.01

Analysis of different PV array configurations affected by POSITION-BASED SHADING PATTERNS:

Array Configuration	Output	Healthy	Corner	Center	L-Shape	Frame	Diagonal
TCT	**Isc (A)**	15.3	15.3	15.3	15.0	13.4	15.0
	Power (W)	1277.4	1161.6	907.7	931.4	653.8	1139.8
	Efficiency (%)	100	90.93	71.05	72.91	51.18	89.22
MS	**Isc (A)**	15.3	15.3	13.4	13.7	13.7	15.0
	Power (W)	1277.3	1196.0	**1061.9**	1038.0	745.5	1139.7
	Efficiency (%)	100	93.63	83.13	81.26	58.36	89.22
DS	**Isc (A)**	15.8	15.8	15.2	13.9	12.3	15.5
	Power (W)	**1317.88**	**1219.9**	1058.7	**1071.2**	**864.1**	**1177.0**
	Efficiency (%)	100	92.57	80.33	81.28	65.57	89.31

For row-wise shading pattern, the array configurations TCT, McSq, and DmSq generated the efficiency of 64.79%, 70.28% and 72.26% respectively. For Column-wise shading pattern, the array configurations TCT, McSq and DmSq generated the efficiency of 71.09%, 70.37% and 61.52% respectively. For diagonal-strip shading pattern, the TCT, McSq, and DmSq array configurations yielded efficiencies of 76.61%, 82.49% and 73.66% respectively. Among these, the McSq configuration achieved the highest efficiency of 74.38%.

For row-wise shading pattern, the array configurations TCT, McSq, and DmSq generated the efficiency of 64.97%, 70.61% and 72.50% respectively. For Column-wise shading pattern, the array configurations TCT, McSq and DmSq generated the efficiency of 71.26%, 70.61% and 61.85% respectively. Under the diagonal-strip shading pattern, the TCT, McSq, and DmSq array configurations achieved efficiencies of 77.64%, 82.68% and 73.93% respectively. Among these, the McSq configuration demonstrated the highest efficiency of 74.63%.

8. CONCLUSION:

This study presents a comprehensive simulation-based evaluation of different PV array configurations using MATLAB/Simulink®. The results indicate that the Magic Square (McSq) configuration consistently delivers superior performance compared to other array arrangements across a range of shading conditions, achieving an average efficiency of 74.38% for monofacial and 74.63% for bifacial systems. The analysis also includes performance metrics such as short-circuit current and power output. Findings suggest that distributing shading more uniformly across the array helps reduce mismatch losses, thereby enhancing overall energy yield. Among the evaluated configurations, both TCT and McSq layouts show effective mitigation of the negative impacts caused by partial shading, with the McSq configuration demonstrating a clear efficiency advantage. These findings offer valuable guidance for selecting optimal PV array designs based on environmental conditions and provide a basis for future research focused on enhancing photovoltaic system performance.

REFERENCES:

[1] S.Serna-Garcés, J.Bastidas-odríguez and C.Ramos-Paja, "Reconfiguration of urban photovoltaic arrays using commercial devices," *Energies,* vol. 9, no. 6 Dec, 2015, p. 1.

[2] B. Parida, S. Iniyan and R. Goic, "A review of solar photovoltaic technologies," *Renew. Sustain. Energy Rev,* vol. 15, no. Apr, 2011, pp. 1625-1636.

[3] K. Lappalainen and S. Valkealahti, "Effects of irradiance transition characteristics on the mismatch losses of different electrical PV array configurations," *IET Renew. Power Gener,* vol. 11, no. Feb, 2017, pp. 248-254.

[4] C. K. J. O. a. K. J. T. Hong, "Nonlinearity analysis of the shading effect on the technical-economic performance of the building integrated photovoltaic blind," *Appl. Energy,* vol. 194, no. May, 2017, pp. 467-480.

[5] M. M. Escribano, M. G. Solano, I. D. P. L. Laita, J. M. Alvarez, L. Marroyo and E. L. Pigueiras, "Module temperature dispersion within a large PV array: Observations at the Amareleja PV Plant,," *IEEE J. Photovolt,* vol. 8, no. Nov, 2018, pp. 1725-1731.

[6] V. Sharma and S. S. Chandel, "A novel study for determining early life degradation of multi-crystalline-silicon photovoltaic modules observed in western Himalayan Indian climatic conditions," *Sol. Energy,* vol. 134, no. Sep, 2016, pp. 32-44.

[7] M. A. M. Ramli, E. Prasetyono, R. W. Wicaksana, N. A. Windarko, K. Sedraoui and Y. A. Al-Turki, "On the investigation of photovoltaic output power reduction due to dust accumulation and weather conditions," *Renew. Energy,* vol. 99, no. Dec, 2016, pp. 836-844.

[8] F.M.Zaihidee, S. Mekhilef, M. Seyedmahmoudian and B. Horan, "Dust as an unalterable deteriorative factor affecting PV panel's efficiency: Why and how," *Renew. Sustain. Energy Rev,* vol. 65, p. 1267–1278, Nov 2016..

[9] V. M. R. Tatabhatla, A. Agarwal and T. Kanumuri, "Improved power generation by dispersing the uniform and non-uniform partial shades in solar photovoltaic array," *Energy Convers. Manage,* vol. 197, Oct, 2019.

[10] C. Deline, S. Ovaitt, M. Gostein, J. Braid, J. Newmiller and I. Suez, "Irradiance Monitoring for Bifacial PV Systems' Performance and Capacity Testing," *IEEE JOURNAL OF PHOTOVOLTAICS,* vol. 14, no. Sep, 2024, pp. 803-814.

[11] I. A. J. C. A. T. a. A. F. Damien Cosme, "Position dependence of the performance gain by selective ground albedo enhancement for bifacial installations," *3Advanced Solar Energy Technologies Consulting BV, 3000 Leuven,* pp. 1-6, 2023.

[12] C. Deline, J. Meydbray and M. Donovan, "Photovoltaic Shading Testbed for Module-Level Power Electronics: 2016 Performance Data Update," National Renewable Energy Laboratory, Golden, Colorodo, Sep, 2016.

[13] A. Mermoud, "PVSyst," 2009. [Online]. Available: https://www.pvsyst.com/.

[14] S. DEVAKIRUBAKARAN, R. VERMA, B. CHOKKALINGAM and L. MIHET-POPA, "Performance Evaluation of Static PV Array Configurations for Mitigating Mismatch Losses," *IEEE,* vol. 11, no. May, 2023, pp. 47725-47749.

[15] V. M. R. Tatabhatla, A. Agarwal and T. Kanumuri, "Improved power generation by dispersing the uniform and non-uniform partial shades in solar photovoltaic array," *Energy Convers. Manage,* vol. 197, Oct, 2019.

[16] S. D. a. C. Bharatiraja, "A novel fused fibonaccigeometric number pattern-based PV array configuration for mitigating the mismatch losses," *Proc. IEEE IAS Global Conf. Renew. Energy Hydrogen Technol. (GlobConHT),* no. March 2023, pp. 1-6, 2023.

[17] D. S. M. S. B. P. K. B. a. L. M.-P. S. Alwar, "Performance analysis of thermal image processing based photovoltaic fault detection and PV array reconfiguration—A detailed experimentation," *Energies,* vol. 15, no. November, 2022, 2022.

[18] S. K. C. K. R. K. N. K. R. M. T. S. B. a. H. H. A. B. P. Kumar, "Performance enhancement of partial shaded photovoltaic system with the novel screw pattern array configuration scheme," *IEEE Access,* vol. 10, no. 2022, pp. 1731-1744, 2022.

[19] P. R. S. S. B. T. a. H. H. A. B. Aljafari, "A zero switch and sensorless reconfiguration approach for sustainable operation of roof-top photovoltaic system during partial shading," *IET Renew. Power Gener,* vol. 17, no. April 2023, pp. 1385-1412, 2023.

[20] S. N. Pappachan, "Hybrid red deer with moth flame optimization for reconfiguration process on partially shaded photovoltaic array," *Energy Sources, Recovery, Utilization, Environ. Effects,* no. February 2022, pp. 1-27, 2022.